Bacteriorhodopsin wildtype and variant aspartate-96 → asparagine as reversible holographic media

Norbert Hampp,* Christoph Bräuchle,* and Dieter Oesterhelt‡
*Institut für Physikalische Chemie, Ludwig-Maximilians Universität München, D-8000 München 2 and ‡Max-Planck Institut für Biochemie, D-8033 Martinsried, Federal Republic of Germany

ABSTRACT Air dried films of purple membranes (PM) from *Halobacterium halobium* containing the photochromic protein bacteriorhodopsin (BR) were prepared and the BR-photocycle of this material analyzed. The absorption maxima of the initial state *B* (λ_{max} = 570 nm) and the photochemical intermediate *M* (λ_{max} = 412 nm), which is the longest living intermediate in suspension ($\tau \approx 10$ ms), were spectrally well separated. Light-induced population gratings between *B* and *M* were used for reversible holographic recording in these dry PM films. The resolution (>5,000 lines/mm) of PM films was comparable to the corresponding values of conventional photochromic recording materials. The longterm stability toward photochemical degradation of PM films is excellent (>100.000 recording cycles). The spectral bandwidth (400–680 nm) of such films covers nearly the whole visible spectrum. Both the photochemical transition from *B* → *M* with wavelengths in the green–red range and from *M* → *B* with blue light were utilized for holographic recording. The latter possibility (*M* → *B*) seems to be advantageous for several applications because the holographic grating is only formed during reconstruction. Higher reading intensities lead to higher population of the *M*-state and result in an increase of the fringe contrast instead of decreasing it. New possibilities for the further development of holographic media based on bacteriorhodopsin are raised by the availability of PM variants with modified optical properties. By the use of the variant BR-326, which differs from the wildtype PM by a single amino acid exchange (aspartate-96 → asparagine), the sensitivity of PM films is increased by ~50% from 12 cm^2/J to 19 cm^2/J for recording with 568 nm. The sensitivity for recording with 413 nm (33 cm^2/J) is not influenced by the amino acid exchange. The observed diffraction efficiency η of PM films with BR-326 is twice that of BR-wildtype (BR-WT) films and is in the range of conventional organic photochromics (≈ 1%). In dried films of both BR-WT and BR-326 the *M*-decay was shown to be at least biexponential.

INTRODUCTION

The purple membrane (PM) from *Halobacterium halobium* consists of a two-dimensional hexagonal lattice of trimers of the photochromic protein bacteriorhodopsin (BR) in a lipid bilayer (1). In the halobacterial cell it acts as a light driven proton pump (2). The BR molecule (MW ≈ 26.000 Dalton) consists of a single polypeptide chain of 248 amino acids forming seven transmembrane α-helices. A retinal molecule linked via a protonated Schiff base to lysine 216 forms the chromophoric group (3). The proton pumping activity of light adapted BR is associated with conformational changes of the BR molecule and its chromophoric group during the so-called photocycle (Fig. 1). Due to the high quantum yield of the primary photochemical step and the high specific absorption of the initial state (ϵ = 63.000 $l \cdot mol^{-1} \cdot cm^{-1}$) the photocycle of BR can be initiated efficiently. Since its discovery (4), nearly two decades of intense research have resulted in a comprehensive knowledge of the biochemical, biophysical, and photophysical properties of this membrane protein (5–7).

The extreme longterm stability of PM toward photochemical degradation provoked quite early ideas for various possible technical applications. Suggestions were made to use PM for the desalination of seawater (8), the conversion of sunlight to electricity (9–12), or as a molecular switch in "biochips" (13–15).

Several groups focused their interests on pure optical applications of bacteriorhodopsin. The very fast time scale of the first events in the BR-photocycle (16) are very attractive for high speed optical storage (17, 18). Most of these ideas have yet to reach a state where the technical applicability can be evaluated in detail and their performance compared with conventional techniques. However, in some special areas like holographic recording (19), optical signal conditioning in interferometry (20), ultrafast photodetection (21), second harmonic generation (22), and four-wave mixing (23) promising optical applications have been presented.

Controlled modifications of the BR-photocycle are an important step to a possible technical use of BR. Substitution of the chromophore by retinal analogues is a tool which can be used to vary the photochemical properties of

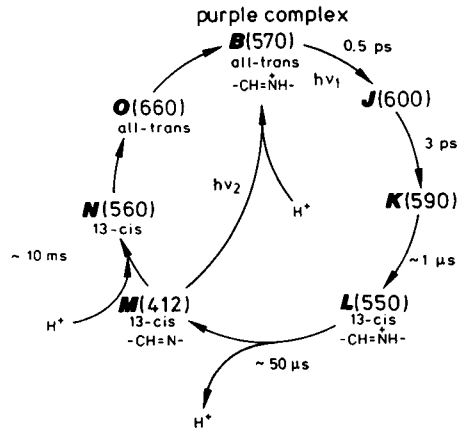

FIGURE 1 Scheme of the photocycle of bacteriorhodopsin. Photointermediates are given by their common short names. Numbers in brackets represent their adsorption maxima. The configuration of the retinal chromophore and the protonation state of the Schiff base are indicated. After excitation with light ($h\nu_1$) BR passes through several intermediates to the *M*-state. From there it can relax either thermally or photochemically ($h\nu_2$) to the initial state *B*. The thermal depopulation of the *M*-state is influenced by the availability of protons. Uptake of a proton is necessary for the reprotonation of the Schiff base. In the case of light-induced transition $M \rightarrow B$, no net proton translocation through the BR-molecule occurs. Therefore, no influence of external proton availability is expected. BR-326 and BR-WT do not differ in the basic characteristics of their photocycles. The photointermediates of BR-326 show the same absorption spectra as BR-WT intermediates.

BR to a high extent (24–27). However, these modified proteins lack the possibility to be produced by conventional biotechnological methods on a large scale.

The generation and isolation of mutated halobacterial strains containing functional variants of PM (28–30) is the key to overcome this problem. New possibilities have arisen to design optimized bacteriorhodopsin-based holographic media which meet the physical demands of the different holographic techniques more specifically. As those PM variants are available in virtually unlimited amounts they are more realistic candidates for technical applications.

In this paper we report on the first use of a functional PM variant (BR-326) as a reversible recording medium for holography. The holographic properties of dry PM films containing BR-wildtype (BR-WT) and the variant BR-326 are compared. Effects caused by the modified photocycle of the BR-326 variant on diffraction efficiency, sensitivity, and hologram decay are discussed. In addition to the recording of holograms by photoexcitation of the initial state *B* ($B \rightarrow M$), purple membrane films offer the possibility of hologram recording with blue light by photoexcitation of the *M*-intermediate ($M \rightarrow B$). It is shown that this new way of hologram recording with the $M \rightarrow B$ photoreaction can have some advantages, especially when it is combined with a reading process in the absorption range of the $B \rightarrow M$ photoreaction.

MATERIAL PREPARATION

Isolation of BR-WT and BR-326 purple membrane suspensions

Purple membrane variants containing mutated bacteriorhodopsins were generated by chemical mutagenesis of *Halobacterium spec. GRB* (31) and isolated by a procedure involving the phototrophic growth behavior of halobacteria with purple membrane of low proton pumping activity (28, 29). A detailed characterization of the isolated mutants, including the strain containing BR-326 is reported by Soppa et al. (30). Wildtype purple membrane (BR-WT) was isolated from *Halobacterium halobium* strain S9. Both PM variants BR-326 and BR-WT were purified according to the procedure given by Oesterhelt and Stoeckenius (4).

BR-326 differs from BR-WT by the replacement of aspartate-96 (Asp96) by asparagine (Asn96). The photointermediates of BR-326 as well as the absorption spectra of light- and dark-adapted initial state *B* are unchanged compared with BR-WT (30); however, the proton pumping activity is nearly lost.

Preparation of purple membrane films

PM films for holography were prepared from concentrated aqueous PM suspension (ph 6–7) on silanized glass plates. PVC-masks were used to define the final shape of the PM film. After drying overnight on air the PVC-masks were removed. The thickness of the films used was 20 μm, having an optical density of $OD_{568} = 1.5$. During measurements, the water content of the PM films was in balance with air at ~60% relative humidity. All experiments were done at room temperature (≈ 23°C).

EXPERIMENTAL

Recording and analyzing plane wave holograms in purple membrane films

It is reasonable to use the simplest hologram, i.e., a plane wave hologram for the characterization of a holographic material. Different techniques with plane wave holograms (32–37) have been developed to extract specific information about the photoreactions and the hologram formation process going on in a holographic medium. The holographic setup used in the experiments here is shown in Fig. 2.

Two plane waves of equal intensity interfere and result in an intensity distribution $I(x)$ along the x-axis

$$I(x) = 2 \cdot I_0 \cdot [1 + \cos(2\pi \cdot x/G)], \quad (1)$$

with a grating period G,

$$G = \lambda_w/(2 \cdot \sin \Theta_w), \quad (2)$$

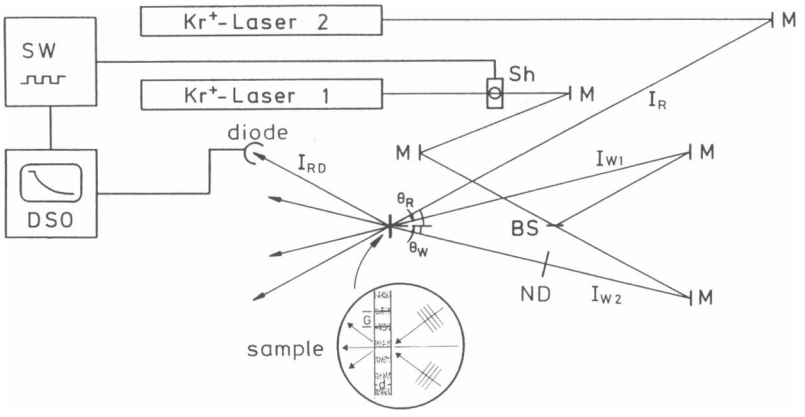

FIGURE 2 Holographic setup for the investigation of purple membrane films. The beam from Kr^+-laser 1 is divided by a beam splitter (BS). The beams I_{w1} and I_{w2} are incident at an angle of $2 \cdot \Theta_w$ on the sample. They are adjusted to equal intensity by means of neutral density filters (ND) to achieve maximal contrast. A photochemically induced holographic grating of thickness d and grating period G is formed in the material (see *insert*) which corresponds to the interference pattern on the sample. Growth and decay of the holographic grating in the PM films are monitored by a reading beam I_R from Kr^+-laser 2 incident at Bragg angle Θ_R. The intensity I_{RD} of the first diffraction order is measured with a calibrated photodetector (diode) and recorded on a digital storage oscilloscope (DSO). The continuous light from the reading beam assures light-adapted BR. The writing beams were switched on and off by a mechanical 1-ms shutter (Sh) that is driven by a tunable controller (SW) and synchronized with the DSO.

where λ_w is the recording wavelength, Θ_w is the half angle between the writing beams, and I_0 is the intensity of one of the recording beams. In the bright parts of the grating (see insert of Fig. 2) a photochemical reaction is induced. The photochemical reaction constants k_i are described by the equation

$$k_i(\lambda) = 2303 \cdot \epsilon(\lambda) \cdot \Phi_{E \to P} \cdot I(\lambda)^z, \tag{3}$$

where $\epsilon(\lambda)$ is the molar absorption coefficient of the educt at the wavelength λ, $\Phi_{E \to P}$ is the quantum yield of the photochemical transition from educt (E) to product (P), $I(\lambda)$ is the light intensity in Einstein $\cdot$ $cm^{-2} \cdot s^{-1}$, and z the number of mechanistically necessary photons (32). If intensity and wavelength of the reading beam can be chosen according to the relation

$$k_R \ll k_W, \tag{4}$$

where k_R and k_w are the photochemical rate constants of the reading (R) and writing beams (W), its influence on the analyzed holographic grating is negligible.

Due to the photochemical reaction in the material a spatial modulation of the refractive index $n(x)$ and the absorption coefficient $a(x)$ is induced.

$$n(x) = n_0 + n_1 \cdot \cos(2\pi \cdot x/G) \tag{5a}$$

$$a(x) = a_0 + a_1 \cdot \cos(2\pi \cdot x/G) \tag{5b}$$

The values n_0 and a_0 represent the average refractive index and absorption coefficient and n_1 and a_1 describe the modulation amplitudes of the refractive index and the absorption coefficient.

Holographic gratings are classified into thick and thin holograms by means of the Q-factor (38)

$$Q = 2\pi \cdot \lambda_w \cdot d/n_0 \cdot G^2, \tag{6}$$

where d is the thickness of the hologram. Furthermore, the grating is characterized by its diffraction efficiency η defined as the ratio between the diffracted intensity I_D and the intensity I_0 of the reading beam (39).

$$\eta = I_D/I_0 \tag{7}$$

Kogelnick (40) derived a relation between the modulation amplitudes of the refractive index and absorption coefficient, respectively, and the diffraction efficiency for thick holograms.

$$\eta = [\sin^2(P) + \sinh^2(A)] \cdot D^2 \tag{8}$$

with

$$P = \frac{\pi \cdot n_1 \cdot d}{\lambda_R \cdot \cos\Theta_R}, A = \frac{a_1 \cdot d}{2 \cdot \cos\Theta_R}, D = \exp\left[-\frac{a_0 \cdot d}{\cos\Theta_R}\right]. \tag{9}$$

For low diffraction efficiencies ($\eta \ll 1$) the previous equation can be approximated by

$$\eta = (P^2 + A^2) \cdot D^2. \tag{10}$$

For the early stages of the hologram formation, and a dominant contribution of the phase grating, it can be shown (32) that the hologram starts to grow quadratically in time t:

$$\eta \propto (k_i \cdot t)^2. \tag{11}$$

To determine the sensitivity of the material the growth curves of the holographic gratings were analyzed. The sensitivity S (41) which is a basic parameter for the comparison of recording materials (42, 43) is defined as the slope of the square root of the diffraction efficiency η plotted vs. the exposure E,

$$\sqrt{\eta} = S \cdot E, \text{ with } E = I \cdot t, \tag{12}$$

where I is the total intensity of the writing beams. For a reversible material like bacteriorhodopsin the initial part of the growth curves is used for the evaluation. There the back reaction is of less importance and mainly a single step photoprocess (e.g., $B \rightarrow M$) is observed.

From the decay curve of a holographic grating, which is observed after turning off the writing beams, the lifetime of photointermediates can be derived. In the case of $\eta \ll 1$, the time dependence of the diffracted intensity $I_D(t)$ is directly proportional to the square of the population of the intermediate state (32) which relaxes in a first-order process with the lifetime τ.

$$I_D(t) \propto \exp^2(-t/\tau) \tag{13}$$

For the evaluation of the experimental data the limited beam size and differing beam diameters of writing and reading beams have to be taken into account. The experimentally observed power densities of the diffracted (P_D) and incident reading beam (P_0) are connected with the diffraction efficiency in the center of the interference pattern of a hologram with mainly phase character by the expression (34),

$$\eta = P_D/P_0 \cdot (1 + 2 \cdot w_R^2/w_W^2), \tag{14}$$

where w_R and w_W are the radii of the reading (R) and writing (W) beams. For reading wavelengths out of the absorption maxima, as used in our experiments, mainly the phase contribution is observed which generally exceeds the effect of the amplitude hologram (33).

RESULTS

Classification of holographic gratings in dry purple membrane films

Experiments were done at a writing angle of $\Theta_W = 16.2°$ both for wavelengths 568 and 413 nm with resulting grating periods of $G_{568} \approx 1$ μm and $G_{413} \approx 0.74$ μm. Q-factors of $Q_{568} \approx 47$ and $Q_{413} \approx 63$ are derived for a grating thickness of $d = 20$ μm and an average refractive index of $n_0 = 1.5$. These estimations approve that for holographic gratings in PM films the theory of volume gratings has to be used for the discussion of the experiments described here.

Decay of holographic gratings and determination of the dominating lifetimes in dry purple membrane films

After excitation with light BR reaches the L-state within ~1 μs (Fig. 1). During the transition from $L \rightarrow M$ a proton is released from the Schiff base. In the thermal relaxation step of the M-state a proton is necessary for the reprotonation of the Schiff base. Therefore, the lifetime of the M-intermediate depends on the internal proton availability in the BR-molecule and may be affected by both the proton concentration outside the molecule and the proton transferring properties inside the protein.

In suspensions of BR-WT and BR-326 it was shown (Miller, A. and D. Oesterhelt, manuscript submitted for publication) that the pH of the medium has almost no influence on the lifetime of the M-state of BR-WT ($\approx$ 10 ms). However, the M-lifetime of BR-326 is strongly dependent on the external proton concentration ($\approx$ 200 ms at pH 5, $\approx$ 20 s at pH 8) (44–46). Therefore, it can be concluded that a loss of the internal proton donor capability resulting from the substitution of Asp96 by Asn leads to a random reprotonation of the Schiff base (47). In dried PM films a severe limitation of proton mobility has to be considered.

We investigated the time-dependent decay of population gratings in dried films at 647 nm and observed an, at least, biexponential decay for both BR-WT and BR-326 (Fig. 3). This characteristic decay was observed for BR-WT also with other techniques (e.g., reference 48). Using the least square fit method, the decay curves can be accurately approximated by the function

$$I_D(t) = F \cdot [P_1 \cdot e^{-2 \cdot t/\tau_1} + P_2 \cdot e^{-2 \cdot t/\tau_2} + C], \tag{14}$$

which consists of two exponential and one constant term. The small constant value C compensates the offset voltage from the photodetector and stray light from the lab. P_1 and P_2 represent the relative contributions of fast (τ_1) and slow (τ_2) relaxation components. The value F is a scaling factor for the conversion of voltage to intensity. The relative contributions of the slow and the fast component and the calculated lifetimes are summarized in Table 1. For P_1 and P_2, and the lifetimes τ_1 and τ_2, no significant dependence on the writing intensities at 568 nm was observed in the range of 27–270 mW/cm^2. To explain the observed biexponential decay either two distinct M-forms have to be assumed, according to Groma and Dancsházy (49) and Groma et al. (50) or a photocycle including more than one photoactive species (51), absorbing at the excitation wavelength 568 nm (e.g., B and N), has to be taken

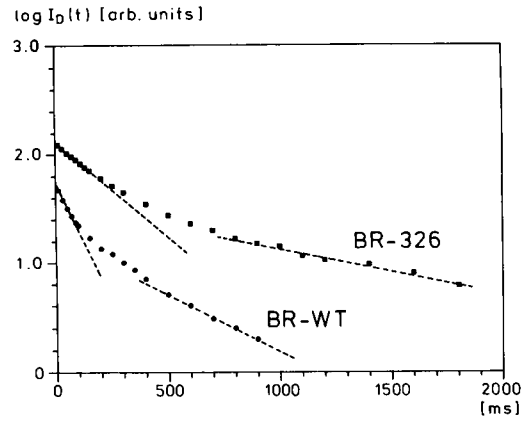

FIGURE 3 Thermal decay of holographic gratings in purple membrane films containing BR-WT and BR-326. Holographic gratings are written with λ_W = 568 nm at an angle of Θ_w = 16.2°. A reading beam of λ_R = 647 nm was used to observe the hologram decay. The logarithm of the diffracted intensity log $I_D(t)$ is plotted vs. time for a decay curve of a hologram written with 54 mW/cm². In the case of a single exponential decay a straight line would be expected. Both BR-WT and BR-326 show minimally biexponential decay.

into account in dry films. Alternatively, a third possibility caused by self-orientation of PM sheets during drying must be considered. It is known that in dry films the flat PM sheets (diam ≈ 500 nm, thickness ≈ 5 nm) are not randomly distributed but are aligned in parallel arrays (19). The proton translocation of a single PM sheet has a vectorial character (from cytoplasm to medium). Two classes of PM sheets are formed during drying, one with the proton translocation vector of the neighbouring PM oriented parallel and one with antiparallel orientation. Because no photoinduced reorientation of PM sheets can occur in dried PM-films this model corresponds to an intensity-independent population distribution between the fast and slow components.

In suspension, the decay of the *M*-state of BR-326 is at least 20 times slower than that of BR-WT (Miller, A., and D. Osterhelt, manuscript submitted for publication). In dry films this factor decreases to 2–3. This result indicates that the limited water content and the low proton mobility in dried PM films has a dominating influence on the lifetime of the *M*-intermediate of both BR-326 and BR-WT (52–55).

TABLE 1 Slow and fast components in the decay curves of dry purple membrane films

	Writing intensity	Fast component		Slow component		Constant	Relative error
	mW/cm²	P_1 %	τ_1 *ms*	P_2 %	τ_2 *ms*	*C* %	%
BR-WT	54	50	98	47	619	3	3.3
BR-326	54	57	300	40	1199	3	1.6

Hologram growth in purple membrane films containing BR-WT and BR-326

Two different methods can be used for hologram recording in PM films. The first method, which has already been introduced (19, 20, 23, 27), use recording wavelengths which induce the photochemical transition of $B \rightarrow M$ (*B*-type holograms). The second method, not previously described, involves the photoinduced transition of $M \rightarrow B$ with blue light (*M*-type holograms). For holograms of the latter type it is necessary to populate the *M*-state by simultaneous illumination with light absorbed by the initial state *B* (520–670 nm).

Sensitivity and diffraction efficiency of *B*-type holograms

Light adaption (30) of the PM films is reached by both a continuous reading beam (e.g., 647 nm) and suitable cycle times of the shutter (0.1 Hz). Depending on the wavelength of the reading beam the growth curves reflect the different contributions of phase and amplitude hologram caused by the *M*/*B*-population grating (Eq. 8). The 647 and 676 nm krypton lines are suitable wavelengths to observe mainly the phase contribution. In Fig. 4, growth curves for BR-WT and BR-326 at a variety of writing intensities are shown. At equal intensities the intensity-dependent steady-state diffraction efficiencies $\eta_S(I)$ for $t \rightarrow \infty$ of BR-326 films are about twice those observed with BR-WT films in all these cases. It is noteworthy that the maximal diffraction efficiency η_{max} of BR-326 is about twice that of BR-WT. A further increase of the intensity leads to a decrease of η due to overexposure. The lifetime of *M* affects the hologram growth at all intensities but the steady-state *M*/*B*-distribution is affected only at nonsaturating intensities. At saturating intensities, where η_{max} is observed, the influence of the *M*-lifetime is of minor importance to the modulation amplitude of the holographic grating. Therefore, the higher maximal diffraction efficiency η_{max} of BR-326 films indicates that the optical, presumably the refractive, properties of BR-326 were modified by the amino acid exchange. For other reading wavelengths (468 and 752 nm) about the same ratio between BR-326 and BR-WT was observed. Based on the initial part of the growth curves, the sensitivity *S* was calculated (Fig. 5) according to Eq. 12. Values taken from all measured curves showed a good correlation. The sensitivity of BR-326 films (S = 19 cm²/J) was ~50% higher than the corresponding value of BR-WT films (S = 12 cm²/J). The sensitivity of BR-WT films, as derived from our experiments, correspond to the value reported by Bunkin et al. (27) if we do not consider the limited, and usually different, diameters of the writing and reading beams.

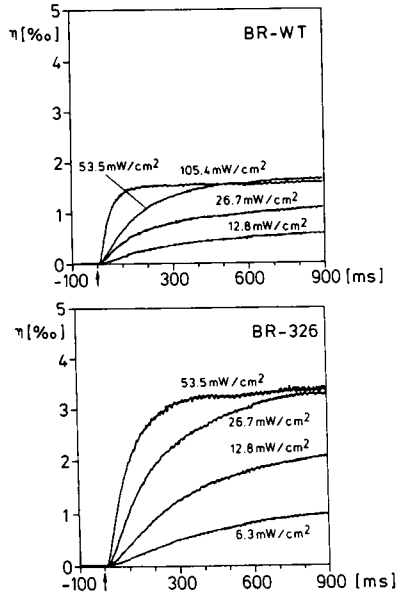

FIGURE 4 Growth curves of *B*-type holograms in dry purple membrane films. Holograms were recorded with λ_W = 568 nm at an angle of Θ_w = 16.2° with laser beams of radius w_W = 1.18 mm at the given intensities in the diagrams. The hologram growth was monitored by a continuous reading beam of λ_R = 647 nm of radius w_R = 1.28 mm at the Bragg angle Θ_R = 18.5° and an intensity I_R = 29.5 mW/cm². The recording beams were turned on at the indicated time (↑). The steady-state diffraction efficiencies $\eta_s(I)$ at the different intensities, as well as the maximal diffraction efficiency η_{max}, observed with BR-326 films (≈0.3%) is about twice that of BR-WT films (≈0.15%). The curves shown were measured with films having an optical density of OD_{568} = 1.5.

Sensitivity and diffraction efficiency of *M*-type holograms

M-type holograms were written with the 413-nm krypton line. Before making the hologram recording, the *M*-state was populated by photoexcitation of the initial state *B* with a pump beam of 568 nm. This pump beam simultaneously serves as the reading beam of the recorded hologram. Because the blue interference pattern induces a holographic population grating (*M*/*B* spatial distribution) in the PM films only under simultaneous illumination with the pump beam, the highest attainable diffraction efficiency depends on the absolute light intensity and the ratio between pumping and writing beams. Furthermore, it is determined by material parameters, e.g., the lifetime of the *M*-intermediate and the optical density of the sample.

In Fig. 6 the influence of different ratios of the intensities of pumping and writing beams on the hologram growth curves and the steady-state diffraction efficiency is shown for PM films containing BR-WT and BR-326. A ratio of ~4:3 between reading (= pumping) (568 nm) and writing intensity (413 nm) gives the highest diffraction

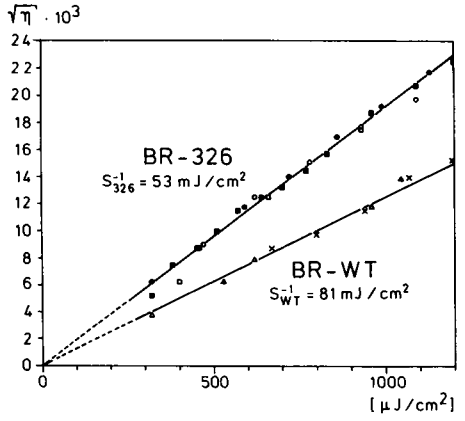

FIGURE 5 Sensitivity of dry purple membrane films containing BR-WT and BR-326 for recording of *B*-type holograms. The sensitivities of BR-WT and BR-326 films were derived from the hologram growth curves shown in Fig. 4. Data points taken from all the different growth curves (indicated by different symbols) show good correlation. The sensitivity of BR-326 films (S = 19 cm²/J) is ~50% higher than the corresponding value of BR-WT films (S = 12 cm²/J). In the figure the commonly used reciprocal sensitivity S^{-1} is shown.

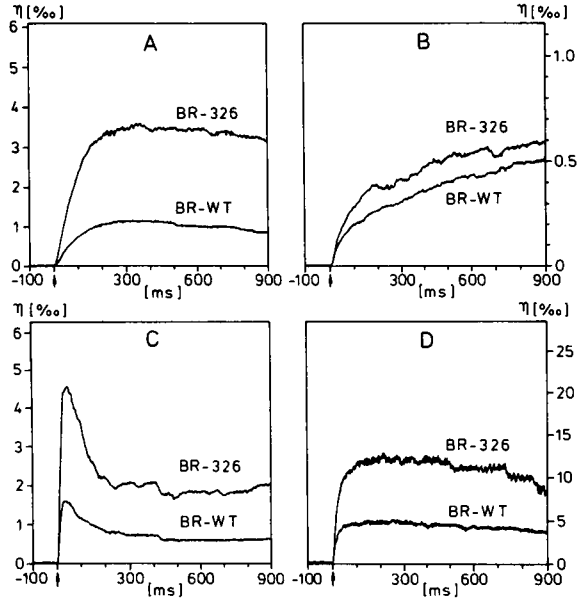

FIGURE 6 Growth curves of *M*-type holograms in dry purple membrane films containing BR-WT and BR-326 at different ratios of writing and reading/pumping intensities. Holograms were recorded in dry PM films having an optical density of OD_{568} = 1.5 at an angle of Θ_W = 16.2° with λ_W = 413 nm. The radii of the writing beams were w_W = 1.25 mm. For pumping and reading of the hologram a beam of λ_R = 568 nm with a radius of w_R = 1.3 mm incident at Bragg angle Θ_R = 22.6° was used. The writing beams were turned on at the indicated time (↑). The dependence of the hologram growth curves on different writing and reading (=pumping) intensities at various ratios are shown. (*A*) I_R = 20 mW/cm², I_W = 15 mW/cm²; (*B*) I_R = 20 mW/cm², I_W = 145 mW/cm²; (*C*) I_R = 210 mW/cm², I_W = 16 mW/cm²; (*D*) I_R = 210 mW/cm², I_W = 150 mW/cm². An optimal ratio is ~4:3 for I_R/I_W (*A* and *D*).

efficiency (Fig. 6, *A* and *D*), which is ≈1% for BR-326 at a reading intensity of 210 mW/cm² (Fig. 6, *D*). Again, this value is twice the value reached with BR-WT films (≈ 0.5%) of equal optical density OD_{568} = 1.5 under identical conditions. The initial overshooting of the diffraction efficiency, which decreases rapidly to a lower stationary level (Fig. 6, *C*), is caused by an imbalance in the ratio between reading and writing intensities ($k_1 \gg k_3$).

In Fig. 7 the sensitivity in *M*-type recording is shown. No difference is observed for the two types of PM films in *M*-type recording up to an exposure of 600 μJ/cm². For higher exposures the curve of BR-WT films enters a nonlinear range. A lower population level of the *M*-state is achieved in BR-WT than in BR-326 films under cw-illumination before recording which corresponds to the shorter *M*-lifetime at the same reading (= pumping) intensities. Due to this lower *M*-concentration the recording with blue light reaches the nonlinear range of hologram growth (saturation) earlier in BR-WT films. A comparison of the sensitivity plots shown in Fig. 5 (*B*-type) and Fig. 7 (*M*-type) shows that the amino acid exchange of Asn96 for Asp96 affected only the thermal relaxation of the BR-molecule and not the photochemical transition from $M \rightarrow B$.

Simulation of the hologram formation in purple membrane films

Due to the intensity-dependent fast photoconversion of $B \rightarrow M$ and the slow thermal relaxation $M \rightarrow B$, a nonsinusoidal shape of the holographic gratings in the PM films is expected even at moderate intensities. To prove this and to check the influence of different *M*-lifetimes the profiles of photochemically induced holographic gratings were calculated numerically. A simplified model of the BR-photocycle was used for the simulations,

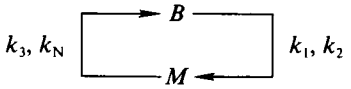

where k_1–k_3 represent the photochemical reaction constants of an interference pattern of writing beams (k_1 : $B \rightarrow M$, k_3 : $M \rightarrow B$) and of a reading beam (k_2) as described in the experimental section. The value k_N corresponds to the thermal relaxation of the *M*-state.

Under the conditions of cw-holography the population density of all intermediates except *M* is very low. The lifetime of *M* in PM film was shown to be in the 0.1–1 s range. Because this value is several orders of magnitudes higher than the lifetime of all other intermediates, *M* is the "bottle-neck" and can be considered to be the dominating intermediate in the population grating. Based on this model the rate equation of the $B \rightleftharpoons M$ system is derived.

$$\dot{B} = -(k_1 + k_2) \cdot B + (k_3 + k_N) \cdot M \qquad (15)$$

Taking into account that after relaxation to the initial state *B* bacteriorhodopsin molecules can start into a new photocycle without any refractory period (56) the equation

$$M(t) = B(0) - B(t) \qquad (16)$$

results. As the probability of a BR-molecule to be in any state other than *B* or *M* is negligible the rate equation for the BR-system is derived,

$$\Rightarrow \dot{B} + k_{123N} \cdot B = k_{3N} \cdot B(0), \qquad (17)$$

where $k_{ij..}$ represents the sum $k_i + k_j + \ldots$.

Steady-state population gratings ($\dot{B} = 0$) in the films are described by

$$B(\infty) = k_{3N}/k_{123N} \cdot B(0). \qquad (18)$$

The dynamics of hologram growth and decay are given by

$$B(t) = C \cdot \exp(-k_{123N} \cdot t) + B(\infty) \cdot [1 - \exp(-k_{123N} \cdot t)], \qquad (19)$$

where the constant *C* has to be determined from a solution of the steady-state expression (Eq. 18) for the growth and the decay of holograms.

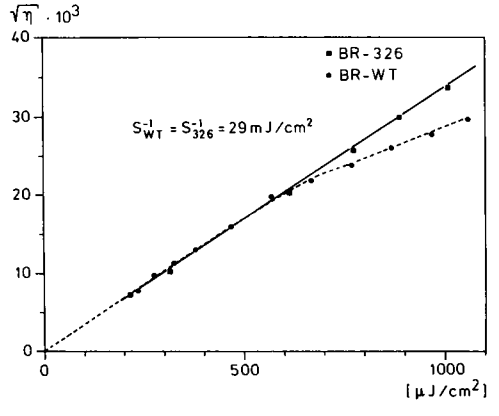

FIGURE 7 Sensitivity of dry purple membrane films containing BR-WT and BR-326 for *M*-type hologram recording. The sensitivity *S* of the PM films was derived according to Fig. 5 from the growth curves shown in Fig. 6, *A* and *D*. The sensitivities of BR-326 and BR-WT films are approximately equal (S = 33 cm²/J) for *M*-type recording. In the figure the commonly used reciprocal sensitivity S^{-1} is given.

The intensity distribution along the x-axis of two interfering Gaussian writing beams is given by

$$I_i(x) = 2 \cdot I_{0i} \cdot e^{-(2 \cdot x^2/w^2)} \cdot [1 + \cos(2\pi \cdot x/G)], \quad (20)$$

where I_{0i} is the maximum intensity in the Gaussian beam profile of the ith component. This has to be taken into account for the overall spatial shape of the population grating.

In Fig. 8 the population distributions of B-type holographic gratings are shown for medium (*top*) and high (*bottom*) writing intensities and average M-lifetimes of BR-WT and BR-326. Obviously the steady-state distributions for these intensities are no longer sinusoidal and the Fourier spectra of the gratings not monochromatic. At moderate writing intensities the longer M-lifetime of BR-326 leads to a directly correlated increase in the grating modulation amplitude. However, at higher intensities broadening of the grating area dominates. Both affect the average background absorption a_0 for the reading beam at wavelengths within the absorption band of the initial state B which weakens the diffracted intensity. Experimentally, the observed higher diffraction efficiency of BR-326 films could not be reached even at high intensities with BR-WT films. Therefore, not only the longer M-lifetime but also different optical properties of BR-WT and BR-326 must be taken into account. Though it is known that the absorption spectra of initial state B and intermediate M are the same for both BR-WT and BR-326 (30), other contributions causing changes in the refractive index (43) have to be considered. In Fig. 9 the growth of a M-type holographic grating is simulated. It can be seen that at the beginning of the growth nearly pure sinusoidal gratings are observed.

For the simulations shown in Figs. 8 and 9 very small writing angles Θ_W and small values for the beam radii had to be assumed to obtain large values of G and a resolvable number of grating spikes. Under these conditions the numerical resolution (2,048 × 1,024 points) allowed accurate simulation of the grating profiles.

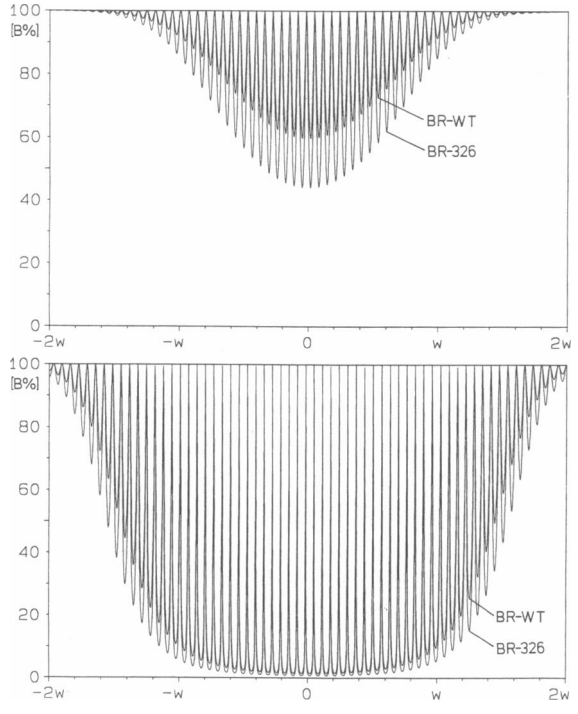

FIGURE 8 Simulation of the shape of steady-state population gratings for B-type hologram recording in purple membrane films containing BR-WT and BR-326. Parameters for the simulation: λ_W = 568 nm, w_W = 0.25 mm, Θ_W = 1.0°, ϵ_W = 63.000 l · mol^{-1} · cm^{-1}, Φ_W = 0.7, τ_M = 350 ms for BR-WT and τ_M = 660 ms for BR-326. (*Top*) I_W = 1 mW/cm^2 (*bottom*) I_W = 100 mW/cm^2. At low intensities the longer M-lifetime of BR-326 leads to a significantly higher modulation amplitude. A slight broadening of the population distribution is observed, mainly at high intensities. The profiles of the gratings at high intensities are of nonsinusoidal shape.

DISCUSSION

PM films containing the variant BR-326 have several advantages compared with BR-WT films with respect to holographic applications. Due to the longer lifetime of M,

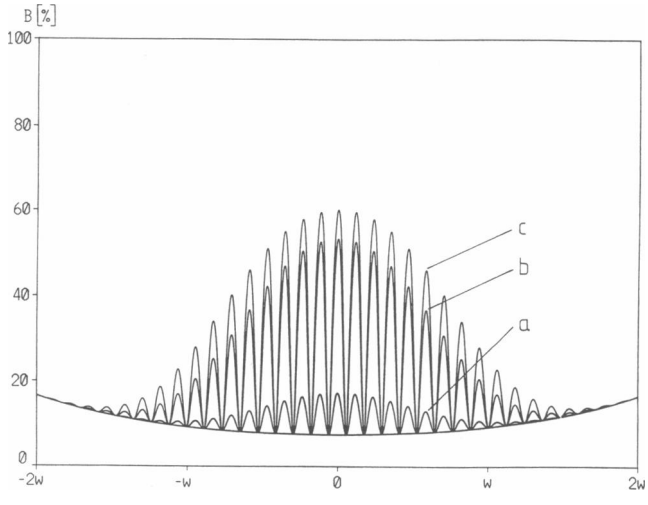

FIGURE 9 Simulation of the growth of a population grating in purple membrane films for recording with blue light (M-type hologram). Parameters for the simulation: λ_W = 413 nm, λ_R = 568 nm, w_W = 0.1 mm, w_R = 0.3 mm, Θ_W = 1.0°, Φ_W = Φ_R = 0.7, τ_M = 150 ms, I_W = 77 mW · cm^{-2}, ϵ_W = 34.000 l · mol^{-1} · cm^{-1}, I_R = 85 mW · cm^{-2}, ϵ_R = 63.000 l · mol^{-1} · cm^{-1}. Time after turning on the writing beams: (*a*) t = 1 ms, (*b*) t = 10 ms, (*c*) t = 1,000 ms. In the beginning the grating has nearly sinusoidal shape. The low average population of the B-state causes low background absorption for the diffracted beam, which can result in a higher diffraction efficiency depending on the reading wavelength of the compared B-type holograms.

significantly higher modulation amplitudes of the *M/B* population distribution can be reached at low intensities. Approximately twice the diffraction efficiency is reached with BR-326 films also at high intensities. Because the absorptive properties of the photointermediates are unchanged, differences in the dispersive behavior of BR-WT and BR-326 have to be assumed. 50% higher sensitivity is observed for the *B*-type recording (BR-WT: 12 cm^2/J, BR-326: 19 cm^2/J) but the same sensitivity is seen with the *M*-type recording (33 cm^2/J). The amino acid exchange in BR-326 affected only the thermal relaxation of the *M*-state but not the properties of the photochemical pathway $M \rightarrow B$. The spectral bandwidth of 400–680 nm is common to both types of BR and the resolution is >5,000 lines/nm. With BR-WT films, 100.000 record/erase cycles were performed without any observable damage to the material.

A further slow-down of the M-decay by several orders of magnitudes, which could be reached if the behavior of BR-326 in suspension (Miller, A., and D. Oesterhelt, manuscript submitted for publication) could be reproduced in films, would supply promising materials for all optical data storage. The most interesting material, a modified BR with unlimited *M*-lifetime, cannot easily be generated by the currently available mutagenesis and selection procedures, but very likely only by genetic engineering of halobacteria. Recording with green light for example, erasure with blue and detection of the recorded information with a wavelength in the near infrared (e.g., 750 nm) where no photochemistry is observed, is the goal of our investigations.

A basic problem in optical recording with reversible photochromic materials is the use of a reading beam with a wavelength similar to that of the writing beams because the same photochemical reactions are induced. Therefore, the fringe contrast of the grating is diminished by increasing reading intensities during reconstruction. The combined use of the photochemical transition $B \rightarrow M$ and $M \rightarrow B$ with two well separated wavelengths allows us to perform "gated" recording with *M*-type holograms. Only in the case of simultaneous pumping with green light for example, allows hologram formation to take place in the material. Again, a population distribution between *M* and *B* is induced, but the diffracted light is absorbed to a lesser extent due to the lower background absorption in the material, which results in a higher diffraction efficiency compared with *B*-type holograms. Under these conditions increasing reading intensities lead to higher diffracted intensities instead of lowering them. In the experiments described here only nonmodulated reading (= pumping) beams were applied. Use of modulated (information carrying) reading and writing beams seems to be a promising approach for future applications like dynamic pattern recognition.

In the reported investigations holography played a dual role. It was used as a scientific tool to study the properties of purple membrane films and at the same time it is a potential technique for technical applications of PM films in holographic storage, real time interferometry and dynamic pattern recognition.

We would like to thank Mrs. S. Meeßen for the isolation of purple membrane suspension. Technical support by the "Consortium für Elektrochemische Industrie," Munich, and fruitful discussions are gratefully acknowledged.

This work was supported by the "Bundesministerium für Forschung und Technologie (BMFT)".

Received for publication 27 November 1989 and in final form 1 March 1990.

REFERENCES

1. Henderson, R., and P. N. T. Unwin. 1975. Three-dimensional model of purple membrane obtained by electron microscopy. *Nature (Lond.).* 257:28–32.
2. Oesterhelt, D., and W. Stoeckenius. 1973. Functions of a new photoreceptor membrane. *Proc. Natl. Acad. Sci. USA.* 70:2853–2857.
3. Lemke, H.-D., and D. Oesterhelt. 1981. Lysine 216 is a binding site of the retinyl moiety in bacteriorhodopsin. *FEBS (Fed. Eur. Biochem. Soc.) Lett.* 128:255–260.
4. Oesterhelt, D., and W. Stoeckenius. 1971. Rhodopsin-like protein from the purple membrane of *Halobacterium halobium. Nature (Lond.).* 233:149–152.
5. Balashov, S. P., and F. Litvin. 1981. Photochemical conversions of bacteriorhodopsin. *Biophys. J.* 26:566–581.
6. Kouyama, P., K. Kinositu, and A. Ikegami. 1988. Structure and function of bacteriorhodopsin. *Adv. Biophys.* 24:123–175.
7. Dunn, R. J., N. R. Hackett, J. M. McCoy, B. H. Chao, K. Kimura, and H. G. Khorana. 1987. Structure-function studies on bacteriorhodopsin. I. Expression of the bacterio-opsin gene in *Escherichia coli. J. Biol. Chem.* 262:9246–9254.
8. Oesterhelt, D. 1976. Bacteriorhodopsin as a light driven ion exchanger? *FEBS (Fed. Euro. Biochem. Soc.) Lett.* 64:20–22.
9. Singh, K., and S. R. Caplan. 1980. The purple membrane and solar energy conversion. *TIBS (Trends Biochem. Sci.).* 5:62–64.
10. Bamberg, E., H.-J. Apell, N. A. Dencher, W. Sperling, H. Stieve, and P. Läuger. 1979. Photocurrents generated by bacteriorhodopsin on planar bilayer membranes. *Biophys. Struct. Mechanism.* 5:277–292.
11. Dér, A., P. Hargittai, and J. Simon. 1985. Time-resolved photoelectric and absorption signals from oriented purple membranes immobilized in gel. *J. Biochem. Biophys. Methods.* 10:295–300.
12. Eisenbach, M., C. Weissmann, G. Tanny, and S. R. Caplan. 1977. Bacteriorhodopsin-loaded charged synthetic membranes. *FEBS (Fed. Eur. Biochem. Soc.) Lett.* 81:77–80.
13. Hong, F. T. 1986. The bacteriorhodopsin model membrane system as a prototype molecular computing element. *Biosystems.* 19:223–236.
14. Karube, I. 1986. Present stage of biochip model development. *Sci. Technol. JPN.* 5:22–24.

15. Mobarry, C., and A. Lewis. 1986. Implementations of neural networks using photoactivated conducting biological materials. *SPIE (Soc. Photo. Instrum. Eng.) J.* 700:304–308.

16. Nuss, M. C., W. Zinth, W. Kaiser, E. Kölling, and D. Oesterhelt. 1985. Femtosecond spectroscopy of the first events of the photochemical cycle in bacteriorhodopsin. *Chem. Phys. Lett.* 117:1–7.

17. Rayfield, G. W. 1989. Bacteriorhodopsin as an ultrafast electrooptic material. *Bull. Am. Phys. Soc.* 34:483.

18. Birge, R. R. 1989. Optical random access memory based on bacteriorhodopsin. *Bull. Am. Phys. Soc.* 34:483.

19. Vsevolodov, N. N., G. R. Ivanitskii, M. S. Soskin, and V. B. Taranenko. 1986. Biochrome films: reversible media for optical recording. *Avtometriia.* 2:41–48.

20. Barmenkov, Y. O., V. V. Zosimov, N. M. Kozhevnikov, O. I. Kotov, L. M. Lyamshev, and V. M. Nikolaev. 1987. Detection of a phase-modulation signal from a fiber-optic interferometer by means of a dynamic hologram in bacteriorhodopsin. *Sov. Phys. Acoust.* 33:334–335.

21. Trissl, H. -W. 1987. Eine biologische Photodiode mit höchster Zeitauflösung. *Optoelektronik Magazin.* 3:105–107.

22. Aktsipetrov, O. A., N. N. Akhmediev, N. N. Vsevolodov, D. A. Esikov, and D. A. Shutov. 1987. Photochromism in the nonlinear otpics—photocontrolled generation of 2nd harmonic by the bacteriorhodopsin molecules. *Dokil. Akad. Nauk USSR.* 293:592–594.

23. Korchemskaya, E. Y., M. S. Soskin, and V. B. Taranenko. 1987. Spatial polarization wavefront reversal under conditions of four-wave mixing in biochrome films. *Sov. J. Quantum Electron.* 17:450–454.

24. Polland, H. -J., M. A. Franz, W. Zinth, W. Kaiser, E. Kölling, and D. Oesterhelt. 1984. Optically picosecond studies of bacteriorhodopsin containing a sterically fixed retinal. *Biochim. Biophys. Acta.* 767:635–639.

25. Kölling, E., W. Gärtner, D. Oesterhelt, and E. Ludger. 1984. Sterically fixed retinal-analogue prevents proton-pumping activity in bacteriorhodopsin. *Angew. Chem. Int. Ed. Engl.* 23:81–82.

26. Gärtner, W., and D. Oesterhelt. 1988. Methoxyretinals in bacteriorhodopsin. Absorption maxima, *cis-trans* isomerization and retinal protein interaction. *Eur. J. Biochem.* 176:641–648.

27. Bunkin, F. V., N. N. Vsevolodov, A. B. Druzhko, B. I. Mitsner, A. M. Prokhorov, V. V. Savranskii, N. V. Tkachenko, and T. B. Shevnenko. 1981. Diffraction efficiency of bacteriorhodopsin and its analogs. *Sov. Tech. Phys. Lett.* 7:630–631.

28. Oesterhelt, D., and G. Krippahl. 1983. Phototrophic growth of halobacteria and its use for isolation of photosynthetically deficient mutants. *Ann. Microbiol. (Inst. Pasteur).* 134*B*:137–150.

29. Soppa, J., and D. Oesterhelt. 1989. Bacteriorhodopsin mutants of *Halobacterium spec. GRB.* 1. The 5-bromo-2'deoxyuridine-selection as a method to isolate point mutants in halobacteria. *J. Biol. Chem.* 264:13043–13048.

30. Soppa, J., J. Otomo, J. Straub, J. Tittor, S. Meeßen, and D. Oesterhelt. 1989. Bacteriorhodopsin mutants of *Halobacterium spec. GRB.* 2. Characterization of mutants. *J. Biol. Chem.* 264:13049–13056.

31. Ebert, K., W. Goebel, and F. Pfeifer. 1984. Homologies between heterogeneous extrachromosomal DNA populations of *Halobacterium halobium* and four new halobacteria isolates. *Mol. Gen. Genet.* 194:91–97.

32. Bräuchle, C., and D. M. Burland. 1983. Holographic methods for the investigation of photochemical and photophysical properties of molecules. *Angew. Chem. Int. Ed. Engl.* 22:582–598.

33. Burland, D. M., and C. Bräuchle. 1982. The use of holography to investigate complex photochemical reactions. *J. Chem. Phys.* 76:4502–4512.

34. Deeg, F. W., J. Pinsl, C. Bräuchle, and J. Voitländer. 1983. The evaluation of photochemical quantum yields by holography. *J. Chem. Phys.* 279:1229–1234.

35. Deeg, F. W., J. Pinsl, and C. Bräuchle. 1986. Investigation of irreversible photochemical reactions by transient grating techniques. *J. Phys. Chem.* 90:5710–5715.

36. Gehrtz, M., J. Pinsl, and C. Bräuchle. 1987. Sensitive detection of phase and absorption gratings: Phase modulated, homodyne detected holography. *Appl. Phys. B.* 43:61–77.

37. Hrebabetzky, F., and C. Bräuchle. 1989. Dynamical-phase-modulated holography (DPMH)—A method for measuring hologram formation mechanisms and the nonlinear refractive index. *IEE (Inst. Elec. Eng.) Conf. Publ.* 311:106–110.

38. Klein, W. R., and B. D. Cook. 1967. Unified approach to ultrasonic light diffraction. *IEEE Trans Sonics & Ultrasonic SU.* 14:123–134.

39. Collier, R. J., C. B. Burckhardt, and L. H. Lin. 1971. Optical Holography. Academic Press, New York. 269–280.

40. Kogelnick, H. 1969. Coupled wave theory for thick hologram gratings. *Bell Syst. Tech. J.* 48:2909–2947.

41. Kurtz, R. L., and R. B. Owen. 1975. Holographic recording materials—a review. *Opt. Eng.* 14:393–401.

42. Pinsl, J., F. W. Deeg, and C. Bräuchle. 1986. Two-photon four-level hologram recording in poly-(alkyl-alpha-cyanoacrylates). *Appl. Phys. B.* 40:77–84.

43. Pinsl, J., M. Gehrtz, A. Reggel, and C. Bräuchle. 1987. Photochemistry of tertiary nitrosoalkanes in solid polymer matrices: a promising new class of organic materials for holographic recording with semiconductor lasers. *J. Am. Chem. Soc.* 109:6479–6486.

44. Gerwert, K., B. Hess, J. Soppa, and D. Oesterhelt. 1989. Role of aspartate-96 in proton translocation by bacteriorhodopsin. *Proc. Natl. Acad. Sci. USA.* 86:410–415.

45. Braiman, M. S., T. Mogi, T. Marti, L. J. Stern, H. G. Khorana and K. J. Rothshild. 1988. Vibrational spectroscopy of bacteriorhodopsin mutants: light-driven proton transport involves protonation changes of aspartic acid residues 85, 96, 212. *Biochemistry.* 27:8516–8520.

46. Holz, M., L. A. Drachev, T. Mogi, H. Otto, A. D. Kaulen, M. P. Heyn, V. P. Skulachev, and H. G. Khorana. 1989. Replacement of aspartic acid-96 by asparagine in bacteriorhodopsin slows both the decay of the M intermediate and the associated proton movement. *Proc. Natl. Acad. Sci. USA.* 86:2167–2171.

47. Tittor, J., C. Soell, D. Oesterhelt, H.-J. Butt, and E. Bamberg. 1989. A defective proton pump, point-mutated bacteriorhodopsin Asp96 → Asn is fully reactivated by azide. *EMBO (Eur. Mol. Biol. Organ.) J.* 8:3477–3482.

48. Váró, G., and L. Keszthelyi. 1983. Photoelectric signals from dried oriented purple membranes of *Halobacterium halobium. Biophys. J.* 43:47–51.

49. Groma, G. I., and Z. Dancsházy. 1986. How many M forms are in the bacteriorhodopsin photocycle? *Biophys. J.* 50:357–366.

50. Groma, G. I., S. L. Helgerson, P. K. Wolber, D. Beece, Z. Dancsházy, L. Keszthelyi, and W. Stoeckenius. 1984. Coupling between the bacteriorhodopsin photocycle and the protomotive force in *Halobacterium halobium* cell envelope vesicles. II. Quantitation and preliminary modeling of the M → bR reactions. *Biophys. J.* 45:985–992.

51. Kouyama, T., and A. Nasuda-Kouyama. 1989. Turnover rate of the proton pumping cycle of bacteriorhodopsin: pH and light-intensity dependences. *Biochemistry*. 28:5963–5970.

52. Dyukova, T. V., N. N. Vsevolodov, and L. N. Chekulayeva. 1985. Change in the photochemical activity of bacteriorhodopsin in polymer matrices on its dehydration. *Biophys. J.* 30:668–672.

53. Korenstein, R., and B. Hess. 1977. Hydration effects on the photocycle of bacteriorhodopsin in thin layers of purple membrane. *Nature (Lond.)*. 270:184–186.

54. Lazarev, Y. A., and E. L. Terpugov. 1980. Effect of water on the structure of bacteriorhodopsin and photochemical processes in purple membranes. *Biochim. Biophys. Acta*. 590:324–338.

55. Kovács, I., and G. Váró. 1988. Charge motion in vacuum-dried bacteriorhodopsin. *J. Photochem. Photobiol. B Biol.* 1:469–474.

56. Dancsházy, Z., G. I. Groma, D. Oesterhelt, and J. Tittor. 1986. The photochemical cycle of bacteriorhodopsin has no refractory period. *FEBS (Fed. Eur. Biochem. Soc.) Lett.* 196:198–202.